**Steady-state growth of an interfacial crack by corrosion**

N A Fleck and J R Willis,

University of Cambridge, UK

26 November 2020

**Abstract**

The Wiener-Hopf technique is used to obtain a 2D steady-state solution for the progressive conversion of a pristine interface into a corroded interface between two dissimilar solids. The interface is of infinite extent, and comprises a semi-infinite pristine portion and a semi-infinite corroded portion. Fickian diffusion of the active species (solute) occurs in the upper half-space, with no diffusion in the lower half-space. Corrosion occurs by chemical reaction between the solute and the top surface of the lower half-space, and the path of solute diffusion involves 3 stages. The solute (i) leaves a solute-rich zone of disbonded and previously corroded interface, (ii) enters into and diffuses through the upper half-space, and (iii) leaves the upper half-space and enters the upstream pristine interface where it reacts with the surface of the lower half-space to produce the corrosion product. A steady state is established: the corrosion front moves at a constant velocity $V$ which is dictated by the critical value of accumulated solute on the interface that is needed to form corrosion product and disbond the interface. The reaction zone directly ahead of the corrosion front has a characteristic length that depends upon the diffusion parameters and front velocity $V$. An asymptotic solution by the Wiener-Hopf analysis is obtained for the diffusion problem at large $V$. Scaling laws emerge and support the predictions of a much simpler 1D physical model.

Keywords: diffusion theory, corrosion, Wiener-Hopf technique, Fourier transforms, interfacial fracture

## 1. Introduction

The corrosion of engineering structures is a common phenomenon with severe economic consequences. A ubiquitous example of wet corrosion is the rusting of steel by water, particularly when the water has a high concentration of dissolved oxygen. The steel may be partially protected against corrosion by the application of a thick coating (made from epoxy for example); diffusion of water can occur through the coating and attack the underlying steel at the interface.

The corrosion product (rust, in the case of steel and water) may adopt a crack-like shape between two bonded, dissimilar solids of steel and epoxy; if this corrosion product allows for the rapid diffusion of the active species (water in the rust) then the corrosion mechanism may resemble crack propagation at an interface. We shall consider this scenario in the present study, see Fig. 1. Specifically, we shall assume that a bulk diffusional path exists for solute diffusion within an upper half-space; the diffusion path connects the flanks of a previously corroded interface (the source of the diffusing species), and a fracture process zone immediately ahead of the tip of the corroded zone (the sink of the diffusing species). Active corrosion is by a chemical reaction between the solute and the lower half-space (for example water on steel), and occurs at the interface within the fracture process zone.

A specific motivation for the present study is the practical problem of adhesively bonding steel parts by an epoxy adhesive in the marine industry. Depending upon the specific design and tolerances, the adhesive layer may be thin (0.1mm or less), or it may have a high thickness (on the order of 10mm). The present study assumes a thick layer of adhesive and represents a first step towards understanding the general phenomenon. Ingress of water into the joint can lead to the nucleation and growth of a water-filled interfacial crack, with transport of oxygen occurring quickly along the water-filled interfacial crack (ie rust layer) and then more slowly by diffusion through the epoxy, see for example Bordes et al. (2009). Thus, the rate limiting steps are diffusion of oxygen within the epoxy and the rate of reaction of the oxygen (and water) with the pristine interface ahead of the crack. The delamination velocity $V$ is dictated by oxygen diffusion under its concentration gradient within the epoxy, from the crack flanks to the fracture process zone.

Additional examples of interfacial corrosion between dissimilar solids by the diffusion of solute within one of the substrates include (i) the corrosion of a ceramic-metallic interface by the diffusion of water within the ceramic, and (ii) hydrogen-induced cracking of a steel-nickel alloy bilayer in nuclear pressure vessels by the diffusion of hydrogen within the steel (Ayas et al. (2015)).

### 1.1 A scaling law for the migration of a steady state corrosion front along an interface

We begin by presenting a simple physical model for the progressive corrosion of an interface between two dissimilar solids, such that diffusion of an active solute species (for example, water) can occur in the upper half-space (for example epoxy), but not in the lower half-space (steel, for example), see Fig. 1. The interface between the two half-spaces corrodes when the active solute species is present at the interface.

Assume that the interface has corroded partially, such that the interface has debonded and the concentration of solute is fixed at the value $C_0$ within the fully corroded portion of the interface. Diffusion of the solute within the upper half-space transports solute from the corroded zone to the intact upstream interface, where it reacts with the underlying half-space at a rate $kC$. Here, $k$ is the mass transfer factor and $C$ is the local volumetric concentration in the upper half-space adjacent to the interface. The interface debonds when the accumulated solute at the interface attains a critical value $Q$ (per unit area of interface) and thereafter the interface contains solute of concentration $C_0$. It is envisaged that the continued feeding of solute occurs without restriction along the corroded interface from the right-hand end of the interface.

A simple scaling argument can be used in order to estimate the steady-state propagation velocity $V$ of the corrosion front, from right to left, in Fig. 1. Assume that after a time $\tau$ solute has diffused a characteristic distance $\bar{d}$ ahead of the corrosion front into the upper half-space; then, then the random-walk equation for diffusion suggests that

$$\bar{d} \approx \sqrt{D\tau} \tag{1.1}$$

where $D$ is the diffusion coefficient of solute within the upper half-space. Dimensional analysis suggests this dependence in the absence of any other physical parameters, regardless of the number of dimensions in the problem. Any numerical pre-factor is dropped as we are only interested in a scaling argument. Now assume that the solute, upon reaching the interface with the lower half-space, reacts at a rate dictated by the volumetric flux rate $j = kC$ at the interface. The quantity of deposited solute over the length $\bar{d}$ in time $\tau$ is on the order of

$$Q\bar{d} \approx kC_0\bar{d}\tau \tag{1.2}$$

The velocity $V = \bar{d} / \tau$ follows immediately from (1.1) and (1.2) as

$$V = \left( \frac{DkC_0}{Q} \right)^{1/2} \tag{1.3}$$

Now consider some representative values for the corrosion of a steel/epoxy interface. Typically, the free corrosion thickening rate $kC_0$ is on the order of 0.1 mm per year = 3.2 x $10^{-12}$ m $s^{-1}$ for steel in salt water (Alcántara et al. (2017)), and the diffusion constant for water in epoxy is on the order of $D$ = 1 x $10^{-13}$ $m^2$ $s^{-1}$ (Bordes et al. (2009)). If we assume that the critical value of accumulated solute to disbond the interface is $Q$=10 nm (Gettings et al. (1977)), then (1.3) suggests that $V$=5.6 $nms^{-1}$, that is 180 mm per year. Thus, $kC_0/V$ is on the order of 5.7 x $10^{-4}$, and assuming that the concentration $C_0$ is on the order of 0.08 (Bordes et al. (2009)), we obtain $k/V$= 0.007. Thus, the diffusion front moves much faster than the rate of free corrosion.

Additional insight is obtained by re-phrasing (1.3) into the non-dimensional form as

$$\frac{k}{V} = \left( \frac{kQ}{DC_0} \right)^{1/2} \tag{1.4}$$

It is clear from (1.4) that the parameter $k/V$ is small provided the critical value of accumulated solute to disrupt the interface $Q$ is small. In the full asymptotic analysis to be presented below, the assumption that $k/V$ is small (since $kQ/DC_0$ is small) leads to a considerable simplification of the treatment. The full analysis also reveals that the scaling (1.4) is accurate.

We also note that, upon eliminating $\tau$ from (1.1) and (1.2), we can obtain an estimate for the characteristic diffusion length $\bar{d}$ as

$$\bar{d} = \frac{D}{V} \tag{1.5}$$

The full asymptotic analysis given below is in support of (1.5) and provides a more precise interpretation of the term 'diffusion length'. Upon substituting the values as given above for $(k, D, C_0, Q)$ we obtain $\bar{d}$ = 18 μm from (1.5), for an epoxy/steel joint. This characteristic length scale is much smaller than the leading dimensions of many practical corrosion problems; consequently, the assumption of an infinite interface between two half-spaces does not impose a severe restriction on the relevance of the analysis presented herein. Recall that the thickness of adhesive layers in large marine applications is typically in the range of 0.1 – 10 mm.

## 2. Statement of problem

The steady-state problem is addressed whereby a corrosion front moves at a constant velocity $V$ by the progressive degradation of an interface ahead of the front by the diffusing solute, see Fig. 1. This is idealised by the diffusion of a solute, of volumetric concentration $C$ within an upper half-space in a fixed Cartesian reference frame $(X,Y)$ at time $t$, see Fig. 2a. The bottom surface of the upper half-space is aligned with $Y$=0 and Fick's law of diffusion applies within the solid, such that $C$ satisfies

$$D\left(\frac{\partial^2 C}{\partial X^2}+\frac{\partial^2 C}{\partial Y^2}\right)=\frac{\partial C}{\partial t}, \quad Y>0 \tag{2.1}$$

in terms of a constant diffusion coefficient $D$. Now assume that a steady state is established for the diffusion problem, such that a moving reference frame $(\bar{x},\bar{y})$ can be introduced (travelling in the $-X$ direction at a velocity $V$). Then, we can re-write $C(X,Y,t)$ as $C(\bar{x},\bar{y})$ where

$$\bar{x}\equiv X+Vt, \quad \bar{y}\equiv Y \tag{2.2}$$

This steady state is established by a suitable choice of boundary conditions along the bottom surface of the half-space ($\bar{y}=0$). It is convenient for the analysis to assume that the imposed concentration profile is of amplitude $C_0$ and decays exponentially with distance $\bar{x}$ over a decay length $1/\bar{a}$ as set by the parameter $\bar{a}$ >0, such that

$$C(\bar{x},0)=C_0\exp(-\bar{a}\,\bar{x}), \quad \bar{x}\geq 0 \tag{2.3a}$$

and

$$\text{normal flux, } j_n=D\frac{\partial C}{\partial \bar{y}}=kC(\bar{x},0), \quad \bar{x}<0 \tag{2.3b}$$

Thus, a concentration boundary condition is prescribed along $\bar{x}\geq 0$. In contrast, a flux boundary condition is assumed along $\bar{x}<0$ such that a volumetric flux of solute leaves the half-space at a rate of $kC$ in terms of the mass transfer factor $k$. To complete the statement of boundary conditions, assume that the concentration $C$ vanishes as $\bar{x}^2+\bar{y}^2\to\infty$.

It is convenient to re-write the diffusion equation (2.1) in terms of the moving co-ordinate system $(\bar{x},\bar{y})$, and then to normalise the variables and relevant parameters by the choice:

$$\bar{x} = \frac{D}{V} x\,, \qquad \bar{y} = \frac{D}{V} y\,, \qquad \bar{a} = \frac{V}{D} a\,, \qquad \phi = \frac{C}{C_0}\,, \qquad c \equiv k/V \tag{2.4}$$

The governing partial differential equation (p.d.e.) (2.1) thereby reduces to

$$\frac{\partial^2 \phi}{\partial x^2} + \frac{\partial^2 \phi}{\partial y^2} - \frac{\partial \phi}{\partial x} = 0\,, \quad y > 0 \tag{2.5}$$

while the boundary conditions (2.3) become

$$\phi(x,0) = \exp(-ax)\,, \quad x \geq 0 \tag{2.6a}$$

and

$$\frac{\partial \phi}{\partial y} = c\phi\,, \quad x < 0 \tag{2.6b}$$

The problem remains to solve for $\phi(x,y)$ for assumed values of ($a$, $c$). Note that the value of velocity $V$ is prescribed via the assumed value of $c$. In reality, a suitable *additional* failure criterion is needed in order to *solve* for $c$. A natural choice is to state that crack advance occurs when the critical value of accumulated solute $Q$ (in units of 1/area) on the interface (at $x = 0^-$) attains a critical value. Make use of (2.3b) to write

$$Q = \int_0^{-\infty} \frac{k}{V} C(\bar{x}, 0)\, d\bar{x} \tag{2.7}$$

and re-phrase into non-dimensional form as

$$q = \frac{kQ}{DC_0} \tag{2.8}$$

Then, upon making use of the scaling relations (2.4), we obtain

$$q = c^2 \int_{-\infty}^{0} \phi(x,0)\, dx \tag{2.9}$$

Note that the right-hand side (r.h.s.) of (2.9) is a function of ($c$, $a$); consequently, for any assumed value of critical solute accumulation $q$, and assumed value of $a$, the value of $c$ (and thereby velocity $V$) can be obtained. We shall greatly simplify the analysis below by considering the practical case where $q$ is sufficiently small that $c << 1$. This has the direct physical interpretation that the velocity $V$ much exceeds the mass transfer factor $k$, as already justified in the Introduction.

## 3. Solution method

The p.d.e. (2.5) is solved by the Fourier transform method along with the Wiener-Hopf technique as follows. The Fourier transform method is employed in order to reduce the p.d.e. (2.5) to an ordinary differential equation (o.d.e.), and the Wiener-Hopf technique is then used to solve the resulting o.d.e., see for example Carrier, Krook and Pearson (2005). We begin by writing the Fourier Transform of $\phi(x,y)$ with respect to *x* as

$$\tilde{\phi}(\lambda,y)=\int_{-\infty}^{\infty}e^{i\lambda x}\phi(x,y)dx \tag{3.1}$$

along with the inverse transform

$$\phi(x,y)=\frac{1}{2\pi}\int_{-\infty}^{\infty}e^{-i\lambda x}\tilde{\phi}(\lambda,y)d\lambda \tag{3.2}$$

Then, for $y>0$, the Fourier transform in *x* of the governing p.d.e. (2.5) becomes

$$\tilde{\phi}_{,yy}-\beta^2\tilde{\phi}=0 \tag{3.3}$$

where a comma in the subscript denotes differentiation and

$$\beta(\lambda)=\lambda^{1/2}(\lambda-i)^{1/2} \tag{3.4}$$

The solution of (3.3) is

$$\tilde{\phi}(\lambda,y)=A(\lambda)e^{-\beta y} \tag{3.5}$$

in terms of the unknown function $A(\lambda)$. Now, the branch cuts of the multi-valued function $\beta(\lambda)$ must be chosen such that, for $y>0$, the function $\phi(x,y)$ is finite. To achieve this, we require that $\tilde{\phi}(\lambda,y)\to 0$ as $\lambda\to\pm\infty$. Thus, the inversion path in the $\lambda$-plane will pass between $\lambda=0$ and $\lambda=i$ (with a branch cut from $\lambda=0$ along the negative imaginary axis, and a branch cut from $\lambda=i$ along the positive imaginary axis of the $\lambda$-plane). This ensures that $\beta(\lambda)$ has positive real part in the strip $\{\lambda:\ \mathrm{Im}(\lambda)\in(0,1)\}$.

We proceed to make use of the boundary conditions along *y*=0 in order to solve for $A(\lambda)=\tilde{\phi}(\lambda,0)$ and thereby $\tilde{\phi}(\lambda,y)$ in (3.5), and then perform the inverse transform to determine

$\phi(x,y)$ via (3.2). To proceed, additively decompose $A(\lambda)$ into a + function $A_+(\lambda)$ which is analytic in the upper half-plane (UHP) and a - function $A_-(\lambda)$ which is analytic in the lower half-plane (LHP) such that

$$A(\lambda) = A_+(\lambda) + A_-(\lambda) \tag{3.6}$$

where

$$A_+(\lambda) = \int_0^\infty e^{i\lambda x}\phi(x,0)dx \tag{3.7}$$

and

$$A_-(\lambda) = \int_{-\infty}^0 e^{i\lambda x}\phi(x,0)dx \tag{3.8}$$

Direct evaluation of $A_+(\lambda)$ is performed by making use of (2.6a) to obtain

$$A_+(\lambda) = \frac{1}{a - i\lambda} \tag{3.9}$$

Now make use of the boundary condition (2.6b) along $x<0$ in order to solve for $A_-(\lambda)$. To do so, introduce an auxiliary function

$$f(x) \equiv \phi_{,y}(x,0) - c\phi(x,0) \tag{3.10}$$

and note that the boundary condition (2.6b) along $x<0$ implies $f(x<0)=0$. The Fourier transform $F(\lambda)$ of $f(x)$ is decomposed additively into $F_+(\lambda)$ and $F_-(\lambda)$ such that

$$F(\lambda) = F_+(\lambda) + F_-(\lambda) \tag{3.11}$$

where

$$F_-(\lambda) = \int_{-\infty}^0 e^{i\lambda x} f(x)dx = 0 \tag{3.12}$$

and

$$F_+(\lambda) = \int_0^\infty e^{i\lambda x} f(x)dx \tag{3.13}$$

Now substitute (3.10) into (3.13), extend the integration path to the whole of the x-axis via (3.12), and make use of (3.5) and (3.6) - (3.9) to obtain

$$F_+(\lambda) = -(\beta + c)\left( A_-(\lambda) + \frac{1}{a - i\lambda} \right) \tag{3.14}$$

At this stage of the development we seek solutions for $F_+(\lambda)$ and $A_-(\lambda)$. Note that these two functions have different domains of analyticity. The Weiner-Hopf procedure requires the factorization of the function $(\beta + c)$ in (3.14) *multiplicatively* into the product of a + function and a – function, such that

$$\beta(\lambda) + c = K_+(\lambda) K_-(\lambda) \tag{3.15}$$

The challenge of obtaining a multiplicative split is delayed to the next section. For now, we assume that such a split exists and can be obtained. Then, (3.14) can be re-written in the form

$$\frac{F_+(\lambda)}{K_+(\lambda)} = -K_-(\lambda) A_-(\lambda) - \frac{K_-(\lambda)}{a - i\lambda} \tag{3.16}$$

We seek to collect all of the + functions on one side of the equation, and the – functions on the other side. To do so, we need to split additively the final term on the r.h.s. of (3.16) into a + function and a – function such that

$$\frac{K_-}{a - i\lambda} = \left( \frac{K_-}{a - i\lambda} \right)_+ + \left( \frac{K_-}{a - i\lambda} \right)_- \tag{3.17}$$

This can be done by a straightforward pole-removal technique such that the left-hand side (l.h.s.) of (3.17) becomes

$$\frac{K_-(\lambda)}{a - i\lambda} = \frac{K_-(-ia)}{a - i\lambda} + \frac{\left( K_-(\lambda) - K_-(-ia) \right)}{a - i\lambda} \tag{3.18}$$

Note that the second term on the r.h.s. has a removable singularity at $\lambda = -ia$. This procedure immediately provides the desired additive split,

$$\left( \frac{K_-}{a - i\lambda} \right)_+ = \frac{K_-(-ia)}{a - i\lambda} \tag{3.19}$$

and

$$\left( \frac{K_-}{a - i\lambda} \right)_- = \frac{\left( K_-(\lambda) - K_-(-ia) \right)}{a - i\lambda} \tag{3.20}$$

The relation (3.16) can then be re-written in the form

$$\frac{F_+}{K_+}+\left(\frac{K_-}{a-i\lambda}\right)_+=-K_-A_--\left(\frac{K_-}{a-i\lambda}\right)_- \tag{3.21}$$

The more explicit calculations of the next section will confirm that a common strip of analyticity exists such that the l.h.s of (3.21) is the analytic continuation of the r.h.s and, further, that each side vanishes as $|\lambda|\to\infty$ in its domain of analyticity. Thus, together, they define an entire function $E(\lambda)$ which tends to zero as $|\lambda|\to\infty$. Consequently, $E(\lambda)$=0 everywhere by Liouville's theorem. Equation (3.21) thereby provides

$$A_-(\lambda)=-\frac{1}{K_-(\lambda)}\left[\frac{\left(K_-(\lambda)-K_-(-ia)\right)}{a-i\lambda}\right] \tag{3.22}$$

The challenge remains to perform the multiplicative split of $K(\lambda)$ into the product of $K_+(\lambda)$ and $K_-(\lambda)$ as stated in (3.15). This is achieved in the following section by making use of the Cauchy integral formula along the lines of section 8.2 of Carrier, Krook and Pearson (2005).

## 4. **The kernel decomposition**

First, substitute (3.4) into (3.15) and re-write it in the form

$$K_+K_-=\lambda^{1/2}(\lambda-i)^{1/2}\left(1+\frac{c}{\lambda^{1/2}(\lambda-i)^{1/2}}\right) \tag{4.1}$$

Upon noting that $\lambda^{1/2}$ is a + function, and $(\lambda-i)^{1/2}$ is a – function, we can re-write $K_+(\lambda)$ as

$$K_+=\lambda^{1/2}L_+ \tag{4.2}$$

and $K_-(\lambda)$ as

$$K_-=(\lambda-i)^{1/2}M_- \tag{4.3}$$

so that the problem of finding $K_+(\lambda)$ and $K_-(\lambda)$ becomes one of finding $L_+(\lambda)$ and $M_-(\lambda)$, respectively, where

$$L_+ M_- = \left( 1 + \frac{c}{\lambda^{1/2} (\lambda - i)^{1/2}} \right) \tag{4.4}$$

Note that $K_+$ and $K_-$, and so also $L_+$ and $M_-$, are non-zero in the strip $\{ \lambda : \mathrm{Im}(\lambda) \in (0,1) \}$ because $\mathrm{Re}(\beta) > 0$ in the strip and $c > 0$. Now take logs of both sides of (4.4) in order to convert the product $L_+ M_-$ into a sum, and recall that $c = k/V << 1$ from the Introduction, to give

$$\ln L_+ + \ln M_- \approx \frac{c}{\lambda^{1/2} (\lambda - i)^{1/2}} \equiv G(\lambda) \tag{4.5}$$

It should be noted that the approximation (4.5) is uniformly valid, with error of order $c^2$, only so long as points in the vicinity of $\lambda = 0$ and $\lambda = i$ are avoided — for instance by restricting $\lambda$ to the strip $\{ \lambda : \mathrm{Im}(\lambda) \in [0.25, 0.75] \}$. The proof is omitted but factorization of (4.5) provides approximations to the exact factors with uniform error of order $c^2$, in any narrower strip, such as $\{ \lambda : \mathrm{Im}(\lambda) \in [0.375, 0.625] \}$. It is natural in the first instance to consider integrals to be defined along a line $\Gamma_1$ just above the real axis, as illustrated in Fig. 3. However, the corresponding integrals can always be evaluated by contour deformation to a line such as $\{ \lambda : \mathrm{Im}(\lambda) = 0.5 \}$, then switching to the uniform approximation corresponding to (4.5) and then deforming back to $\Gamma_1$. A corresponding comment applies also to a line $\Gamma_2$ just below $\lambda = i$. For simplicity of presentation, we proceed formally, without further reference to these technicalities.

Recall from section 3 that $G(\lambda)$ has a branch cut from $\lambda = 0$ that extends along the negative imaginary axis, and a branch cut from $\lambda = i$ that extends along the positive imaginary axis of the $\lambda$-plane, see Fig. 3. It is convenient to split the r.h.s. of (4.5) into a + function $G_+$ (that is analytic above the real axis of the $\lambda$-plane, labelled $\Gamma_1$), and a – function $G_-$ (that is analytic below a line $\Gamma_2$ introduced above). Then, $G_+$ can be identified with $\ln L_+$, and $G_-$ can be identified with $\ln M_-$. The functions $G_+$ and $G_-$ are obtained via the Cauchy integral formula as follows. Recall that, for any path $\Gamma$ that encloses $\lambda$ but does not enclose any singularities of an analytic function $G(z)$, the Cauchy integral formula states

$$G(\lambda) = \frac{1}{2\pi i} \int_\Gamma \frac{G(z)}{z - \lambda} dz \tag{4.6}$$

Choose $\Gamma$ to comprise a lower contour from $-\infty$ to $\infty$ along $\Gamma_1$ as defined above, an upper contour $\Gamma_2$ from $\infty$ to $-\infty$ and end segments to close the contour at infinity. Then, the integral in *z* along $\Gamma_1$ (from left to right)

$$\frac{1}{2\pi i}\int_{\Gamma_1}\frac{G(z)}{z-\lambda}dz \tag{4.7}$$

defines the + function $G_+(\lambda)$, whereas the integral in *z* along $\Gamma_2$ (from right to left)

$$\frac{1}{2\pi i}\int_{\Gamma_2}\frac{G(z)}{z-\lambda}dz \tag{4.8}$$

defines the - function $G_-(\lambda)$. Standard methods of contour integration then provide

$$G_+(\lambda)=\frac{c}{i\pi\lambda^{1/2}(\lambda-i)^{1/2}}\ln\left(\frac{\lambda^{1/2}-(\lambda-i)^{1/2}}{\lambda^{1/2}+(\lambda-i)^{1/2}}\right) \tag{4.9a}$$

and

$$G_-(\lambda)=\frac{c}{i\pi\lambda^{1/2}(\lambda-i)^{1/2}}\ln\left(\frac{(\lambda-i)^{1/2}+\lambda^{1/2}}{(\lambda-i)^{1/2}-\lambda^{1/2}}\right) \tag{4.9b}$$

with the immediate result that

$$K_+(\lambda)=\lambda^{1/2}\exp\left(G_+(\lambda)\right)=\lambda^{1/2}\left(\frac{\lambda^{1/2}-(\lambda-i)^{1/2}}{\lambda^{1/2}+(\lambda-i)^{1/2}}\right)^{\frac{c}{i\pi\lambda^{1/2}(\lambda-i)^{1/2}}} \tag{4.10a}$$

and

$$K_-(\lambda)=(\lambda-i)^{1/2}\exp\left(G_-(\lambda)\right)=(\lambda-i)^{1/2}\left(\frac{(\lambda-i)^{1/2}+\lambda^{1/2}}{(\lambda-i)^{1/2}-\lambda^{1/2}}\right)^{\frac{c}{i\pi\lambda^{1/2}(\lambda-i)^{1/2}}} \tag{4.10b}$$

The appendix provides an explicit demonstration of the validity of equations (4.10a,b) by considering the structure of the functions $G_+$ and $G_-$ in order for (4.5) to be satisfied.

We proceed to make use of the expression (4.10b) in order to determine $A(\lambda)$. With $A_-(\lambda)$ given by (3.22), and $A_+(\lambda)$ expressed by (3.9) we obtain

$$A(\lambda) = A_+(\lambda) + A_-(\lambda) = \frac{K_-(-ia)}{(a - i\lambda)K_-(\lambda)} \tag{4.11}$$

We then substitute for $K_-(\lambda)$ from (4.10b). The concentration distribution $\phi(x, y)$ in physical space follows by taking the inverse Fourier transform (3.2) of $\tilde{\phi}(\lambda, y)$, where $\tilde{\phi}(\lambda, y)$ is stated in terms of $A(\lambda)$ in (3.5). The resulting inverse transform reads

$$\phi(x, y) = \frac{K_-(-ia)}{2\pi} \int_{-\infty}^{\infty} \frac{e^{-i\lambda x} \exp\left(-\lambda^{1/2}(\lambda - i)^{1/2} y\right)}{(a - i\lambda)K_-(\lambda)} d\lambda \tag{4.12}$$

The pre-factor $K_-(-ia)$ is obtained by taking the limit of (4.10b) as $\lambda \to -ia$, to give

$$K_-(-ia) = e^{-i\pi/4}(1+a)^{1/2} \left( \frac{(1+a)^{1/2} + a^{1/2}}{(1+a)^{1/2} - a^{1/2}} \right)^{\frac{c}{\pi a^{1/2}(1+a)^{1/2}}} \tag{4.13}$$

## 5. **Evaluation of the concentration profile**

We proceed to evaluate the concentration profile by performing the inverse Fourier transform (4.12) along the path $\Gamma_1$ as shown in Fig. 3 (and as defined previously). Note that the integrand of (4.12) has a pole at $\lambda = -ia$ and branch points at $\lambda = 0$ and $\lambda = i$. We consider two cases in turn: $x < 0$ and $x > 0$.

### 5.1 The case $x < 0$

We deform the contour $\Gamma_1$ into $C_1 - C_4$ in Fig. 3a, and note immediately that the integrand along $C_1$ tends to zero at infinity; consequently, the integral vanishes by Jordan's lemma for $x < 0$. This leaves the keyhole contour $C_2 - C_4$. Write

$$\lambda = i + \rho e^{i\theta} \tag{5.1}$$

along $C_2$, $C_3$ and $C_4$. The contribution to the integral (4.12) from the contour $C_3$ vanishes as the integrand decays to zero sufficiently rapidly as $\rho \to 0$. The contribution from $C_2$ is obtained by

taking $\theta = -3\pi/2$ in (5.1) and by varying $\rho$ from $\rho = \infty$ to $\rho = 0$. Consequently, along $C_2$ we can rephrase $G_-(\lambda)$ of (4.9b), and $K_-(\lambda)$ of (4.10b) as

$$G_-(\lambda) = \frac{c}{\pi\rho^{1/2}(1+\rho)^{1/2}}\left[i\pi + \ln\left(\frac{(1+\rho)^{1/2} - \rho^{1/2}}{(1+\rho)^{1/2} + \rho^{1/2}}\right)\right] \tag{5.2}$$

and

$$K_-(\lambda) = -\rho^{1/2} e^{i\left(\frac{\pi}{4} + \frac{c}{\rho^{1/2}(1+\rho)^{1/2}}\right)}\left(\frac{(1+\rho)^{1/2} - \rho^{1/2}}{(1+\rho)^{1/2} + \rho^{1/2}}\right)^{\frac{c}{\pi\rho^{1/2}(1+\rho)^{1/2}}}, \tag{5.3}$$

respectively. In similar fashion, the contribution from $C_4$ is obtained by taking $\theta = \pi/2$ in (5.1) and varying $\rho$ from $\rho = 0$ to $\rho = \infty$. Along $C_4$ we can rephrase $G_-(\lambda)$ of (4.9b), and $K_-(\lambda)$ of (4.10b) as

$$G_-(\lambda) = \frac{-c}{\pi\rho^{1/2}(1+\rho)^{1/2}}\left[i\pi + \ln\left(\frac{(1+\rho)^{1/2} + \rho^{1/2}}{(1+\rho)^{1/2} - \rho^{1/2}}\right)\right] \tag{5.4}$$

and

$$K_-(\lambda) = \rho^{1/2} e^{i\left(\frac{\pi}{4} - \frac{c}{\rho^{1/2}(1+\rho)^{1/2}}\right)}\left(\frac{(1+\rho)^{1/2} - \rho^{1/2}}{(1+\rho)^{1/2} + \rho^{1/2}}\right)^{\frac{c}{\pi\rho^{1/2}(1+\rho)^{1/2}}}, \tag{5.5}$$

respectively. We note in passing that the expression for $G_-(\lambda)$ in (5.4) is the complex conjugate of that for $G_-(\lambda)$ in (5.2). Now make use of (5.3) and (5.5) in order to evaluate (4.12) along paths $C_2$ and $C_4$. The result is

$$\phi(x,y) = \frac{1}{\pi} e^{i\pi/4} K_-(-ia) \int_0^\infty \frac{e^{(1+\rho)x}}{(1+a+\rho)\rho^{1/2}}\left(\frac{(1+\rho)^{1/2} + \rho^{1/2}}{(1+\rho)^{1/2} - \rho^{1/2}}\right)^{\frac{c}{\pi\rho^{1/2}(1+\rho)^{1/2}}} \cos\left(\frac{c - y\rho(1+\rho)}{\rho^{1/2}(1+\rho)^{1/2}}\right) d\rho \tag{5.6}$$

where $K_-(-ia)$ is given by (4.13).

Recall that the non-dimensional velocity $c$ is related to a critical deposition $q$ by (2.9). Upon substituting (5.6) into (2.9) and switching the order of integration we obtain

$$q=\frac{1}{\pi}c^2e^{i\pi/4}K_-\left(-ia\right)\int_0^\infty\frac{1}{\left(1+\rho\right)\left(1+a+\rho\right)\rho^{1/2}}\left(\frac{\left(1+\rho\right)^{1/2}+\rho^{1/2}}{\left(1+\rho\right)^{1/2}-\rho^{1/2}}\right)^{\frac{c}{\pi\rho^{1/2}\left(1+\rho\right)^{1/2}}}\cos\left(\frac{c}{\rho^{1/2}\left(1+\rho\right)^{1/2}}\right)d\rho \tag{5.7}$$

The limit of $a\to 0$ is the practical case such that the concentration is spatially uniform at $C=C_0$ along $x > 0$. In this limit, $K_-\left(-ia\right)$, as given by (4.13), simplifies to

$$K\left(-i0\right)=e^{(2c/\pi)-(i\pi/4)} \tag{5.8}$$

Consequently, $\phi\left(x,y\right)$ in (5.6) and $q$ in (5.7) simplify to

$$\phi\left(x,y\right)=\frac{1}{\pi}e^{(2c/\pi)}\int_0^\infty\frac{e^{(1+\rho)x}}{\left(1+\rho\right)\rho^{1/2}}\left(\frac{\left(1+\rho\right)^{1/2}+\rho^{1/2}}{\left(1+\rho\right)^{1/2}-\rho^{1/2}}\right)^{\frac{c}{\pi\rho^{1/2}\left(1+\rho\right)^{1/2}}}\cos\left(\frac{c-y\rho\left(1+\rho\right)}{\rho^{1/2}\left(1+\rho\right)^{1/2}}\right)d\rho \tag{5.9a}$$

and

$$q=\frac{1}{\pi}c^2e^{(2c/\pi)}\int_0^\infty\frac{1}{\left(1+\rho\right)^2\rho^{1/2}}\left(\frac{\left(1+\rho\right)^{1/2}+\rho^{1/2}}{\left(1+\rho\right)^{1/2}-\rho^{1/2}}\right)^{\frac{c}{\pi\rho^{1/2}\left(1+\rho\right)^{1/2}}}\cos\left(\frac{c}{\rho^{1/2}\left(1+\rho\right)^{1/2}}\right)d\rho\,, \tag{5.9b}$$

respectively. A numerical evaluation of the integral

$$I_q\left(c\right)=\int_0^\infty\frac{1}{\left(1+\rho\right)^2\rho^{1/2}}\left(\frac{\left(1+\rho\right)^{1/2}+\rho^{1/2}}{\left(1+\rho\right)^{1/2}-\rho^{1/2}}\right)^{\frac{c}{\pi\rho^{1/2}\left(1+\rho\right)^{1/2}}}\cos\left(\frac{c}{\rho^{1/2}\left(1+\rho\right)^{1/2}}\right)d\rho \tag{5.9c}$$

for $c << 1$ reveals that it has the asymptotic form

$$I_q\left(c\right)\approx\frac{\pi}{2}-2.36c \tag{5.9d}$$

which is accurate to within 1% for $c < 0.1$. Consequently, to an excellent approximation (5.9b) gives $q\approx c^2/2$. This supports the simple estimate $q\approx c^2$ of (1.4), except for the factor of 2 that emerges from the full calculation.

### 5.2 The case $x > 0$

Now perform the inverse Fourier transform (4.12) along the path $\Gamma_1$ as shown in Fig. 3b. We deform the contour $\Gamma_1$ into the union of $\mathrm{P}_1$ to $\mathrm{P}_6$, and note that the integral along $\mathrm{P}_1$ vanishes at infinity by Jordan's lemma for $x > 0$. This leaves the contributions from the keyhole contour $\mathrm{P}_2$ to $\mathrm{P}_6$ to be evaluated. A branch point of the integrand of (4.12) exists at $\lambda = 0$, with a branch cut along the negative imaginary axis, as shown in Fig. 3b. Also, a simple pole exists at $\lambda = -ia$. Upon shrinking the radius of the contour $\mathrm{P}_4$ to zero, we find that there is no contribution to the integral (4.12) from the segment $\mathrm{P}_4$. Now write

$$\lambda = \rho e^{i\theta} \tag{5.10}$$

centred on the origin, and proceed to evaluate (4.12) along $\mathrm{P}_2$. The contribution to the contour integral in (4.12) along $\mathrm{P}_2$ reads

$$I_{P_2} = \frac{1}{2\pi} K_-(-ia) \int_{\mathrm{P}_2} \frac{e^{-i\lambda x} \exp\left(-\lambda^{1/2}(\lambda - i)^{1/2} y\right)}{(a - i\lambda) K_-(\lambda)} d\lambda \tag{5.11}$$

where $K_-(-ia)$ is given by (4.13). Along $\mathrm{P}_2$, take $\theta = 3\pi/2$ in (5.10) and vary $\rho$ from $\rho = \infty$ to $\rho = 0$. Then, along $\mathrm{P}_2$ (4.10b) simplifies to

$$K_-(\lambda) = e^{-i\pi/4}(1+\rho)^{1/2} \left( \frac{(1+\rho)^{1/2} + \rho^{1/2}}{(1+\rho)^{1/2} - \rho^{1/2}} \right)^{\frac{c}{\pi\rho^{1/2}(1+\rho)^{1/2}}} \tag{5.12}$$

and (5.11) becomes

$$I_{P_2} = \frac{-i}{2\pi} e^{i\pi/4} K_-(-ia)\, PV \int_0^\infty \frac{e^{-\rho x}\, \mathrm{e}^{-i\rho^{1/2}(1+\rho)^{1/2} y}}{(\rho - a)(1+\rho)^{1/2}} \left( \frac{(1+\rho)^{1/2} - \rho^{1/2}}{(1+\rho)^{1/2} + \rho^{1/2}} \right)^{\frac{c}{\pi\rho^{1/2}(1+\rho)^{1/2}}} d\rho \tag{5.13}$$

where *PV* denotes the Cauchy principal value.

In similar fashion, along $\mathrm{P}_5$ we take $\theta = -\pi/2$ in (5.10) and vary $\rho$ from to $\rho = 0$ to $\rho = \infty$. Then, the contribution to the contour integral in (4.12) along $\mathrm{P}_5$ reads

$$I_{P_5} = \frac{i}{2\pi} e^{i\pi/4} K_-(-ia)\, PV \int_0^\infty \frac{e^{-\rho x}\, \mathrm{e}^{-i\rho^{1/2}(1+\rho)^{1/2} y}}{(\rho - a)(1+\rho)^{1/2}} \left( \frac{(1+\rho)^{1/2} - \rho^{1/2}}{(1+\rho)^{1/2} + \rho^{1/2}} \right)^{\frac{c}{\pi\rho^{1/2}(1+\rho)^{1/2}}} d\rho \tag{5.14}$$

Addition of the contributions $I_{P_2}$ and $I_{P5}$ gives a net contribution that is real, and of magnitude

$$I_{P_2}+I_{P_5}=\frac{-1}{\pi}e^{i\pi/4}K_{-}(-ia)PV\int_0^{\infty}\frac{e^{-\rho x}\sin\left(\rho^{1/2}(1+\rho)^{1/2}y\right)}{(\rho-a)(1+\rho)^{1/2}}\left(\frac{(1+\rho)^{1/2}-\rho^{1/2}}{(1+\rho)^{1/2}+\rho^{1/2}}\right)^{\frac{c}{\pi\rho^{1/2}(1+\rho)^{1/2}}}d\rho \tag{5.15}$$

The final step is to evaluate the contributions to the contour integral in (4.12) along $\mathrm{P}_3$ and $\mathrm{P}_6$. As the radius of the contour $\mathrm{P}_3$ shrinks to zero about the pole at $\lambda=-ia$, the contribution $I_{P3}$ equals $-\pi i$ times the residue of the integrand at $\lambda=-ia$, giving

$$I_{P3}=\frac{1}{2}e^{-ax}e^{-ia^{1/2}(1+a)^{1/2}y} \tag{5.16}$$

In similar fashion we obtain

$$I_{P6}=\frac{1}{2}e^{-ax}e^{ia^{1/2}(1+a)^{1/2}y} \tag{5.17}$$

and consequently,

$$I_{P3}+I_{P6}=e^{-ax}\cos\left(a^{1/2}(1+a)^{1/2}y\right) \tag{5.18}$$

It remains to sum (5.15) and (5.18) to obtain,

$$\phi(x,y)=\frac{-1}{\pi}e^{i\pi/4}K_{-}(-ia)PV\int_0^{\infty}\frac{e^{-\rho x}\sin\left(\rho^{1/2}(1+\rho)^{1/2}y\right)}{(\rho-a)(1+\rho)^{1/2}}\left(\frac{(1+\rho)^{1/2}-\rho^{1/2}}{(1+\rho)^{1/2}+\rho^{1/2}}\right)^{\frac{c}{\pi\rho^{1/2}(1+\rho)^{1/2}}}d\rho$$

$$+e^{-ax}\cos\left(a^{1/2}(1+a)^{1/2}y\right) \qquad ,x>0 \tag{5.19}$$

with the small simplification in the limit $a\to 0$ to

$$\phi(x,y)=1-\frac{1}{\pi}e^{2c/\pi}\int_0^{\infty}\frac{e^{-\rho x}\sin\left(\rho^{1/2}(1+\rho)^{1/2}y\right)}{\rho(1+\rho)^{1/2}}\left(\frac{(1+\rho)^{1/2}-\rho^{1/2}}{(1+\rho)^{1/2}+\rho^{1/2}}\right)^{\frac{c}{\pi\rho^{1/2}(1+\rho)^{1/2}}}d\rho \tag{5.20}$$

## 6. Numerical Evaluation

It remains to evaluate $\phi(x,y)$ by performing the inverse Fourier transform of $\tilde{\phi}(\lambda,y)$ for selected values of *a* and *c*. First, we determine the relation between *c* and *q*, via evaluation of (5.7) by MATLAB standard quadrature methods; the results are given in Fig. 4, for the choices $a$ =0 and 1. The approximation $q = c^2/2$ for $a = 0$ is indistinguishable to the plot shown in Fig. 4 and is thereby omitted; the effect of an increase in *a* from 0 to 1 is to decrease the value of *q* by approximately 17% for any value of *c*: the two curves in the log-log plot of Fig. 4 lay parallel to each other but with a small vertical shift upon changing the value of *a*.

The concentration profile along the interface $\phi(x,0)$ is almost insensitive to the value of *c*, see Fig. 5a obtained by evaluating (5.9a) for $a = 0$. In order to gain insight into the role played by the concentration profile within the corroded interface ($x > 0$), predictions of $\phi(x,0)$ are shown in Fig. 5b for *a* in the range 0 to 100, for the representative choice $c = 0.01$. The concentration profile ahead of the corrosion front (that is, along ($x < 0$)) is remarkably insensitive to the concentration profile behind the corrosion front, as parameterised by *a*. This implies that the main source of solute diffusion is from the corroded layer in the immediate vicinity of the corrosion front, at small positive values of *x*. The velocity of the corrosion front, as parameterised by *c*, depends upon *q* but is relatively insensitive to the concentration profile within the interface that has already corroded (as parameterised by *a*).

Note that (1.5) suggests that the non-dimensional diffusion length *d* is of magnitude

$$d = \frac{V\bar{d}}{D} = 1 \tag{6.1}$$

ahead of the corrosion front. The full calculation supports this scaling law. At $x = -d = -1$, the local concentration equals $\phi(-1,0) = 0.15$ for *c*=0.001-0.01. We conclude that the scaling law (1.5) is accurate: at a distance $\bar{d}$ ahead of the corrosion front the local concentration has dropped to a level of $0.15C_0$ (for the choice $a = 0$, that is $C = C_0$ behind the corrosion front).

Contours plots of $\phi(x,y)$ are given in Fig. 6 for (a) *a*=0, and (b) *a*=1, with *c*=0.01. Numerical experimentation for $0 < c \le 0.1$ revealed that the value of *c* has a negligible effect upon the distribution of $\phi(x,y)$, and so there is no need to include contour plots of $\phi(x,y)$ for other choices of *c*. Note from Fig. 6 that the contours of concentration $\phi(x,y)$ meet the interface along $x < 0$ in an almost perpendicular manner. This is anticipated by the boundary condition (2.6b) for

small $c$. This feature suggests that the simple (1D) scaling laws of the introduction are likely to be accurate: flow of the solute is close to one-dimensional in nature directly ahead of the corrosion front. It is clear from Fig. 6 that $\phi(x, y)$ directly ahead of the corrosion front is only mildly sensitive to the value of $a$. This is consistent with the findings already reported in Figs. 4 and 5.

## 7. Concluding remarks

The present study considers the simplest case of interfacial corrosion dictated by a combination of Fickian diffusion within an upper half-space and simple reaction kinetics on the intact portion of the interface (as modelled by a flux boundary condition for the solute emanating from the upper half-space). When the feeding of solute along the corroded interface behind the corrosion front is much faster than the above kinetic processes the concentration is uniform behind the corrosion front, and $a$=0. Each of the above assumptions need to be verified for each corrosion problem under consideration.

The full 2D asymptotic solution of steady state interfacial corrosion by the Wiener-Hopf technique supports the simple scaling laws developed in the Introduction. Our study also highlights the sensitivity of the steady-state velocity $V$ of corrosion front to the critical value of deposited solute $Q$ required to fail the intact interface. The formula

$$V = \left( \frac{DkC_0}{2Q} \right)^{1/2} \tag{7.1}$$

is accurate for $c < 0.1$ and $0 < a < 1$, and differs from the scaling law (1.3) only by the addition of a factor of $\sqrt{2}$ in the denominator. The independence of $V$ to the parameter $a$ in (7.1) suggests that the above model has applicability to the case of a short corrosion zone in the vicinity of a free boundary. A full computational study is underway for a finite domain, and for any value of $c$.

## Acknowledgements

This project has received funding from the Interreg 2 Seas programme 2014-2020 cofunded by the European Regional Development Fund under subsidy contract No. 03-051. NAF would also like to acknowledge financial support from the European Research Council in the form of an Advanced Grant (MULTILAT, 669764).

## Appendix. Structure of the functions $G_+$ and $G_-$

The functions $G_-$ and $G_+$ can be expressed as follows:

$$G_-(\lambda) = \frac{c}{i\pi\lambda^{1/2}(\lambda - i)^{1/2}}\{\ln(\zeta_1) - \ln(\zeta_2)\},$$

$$G_+(\lambda) = \frac{c}{i\pi\lambda^{1/2}(\lambda - i)^{1/2}}\{\ln(\zeta_3) - \ln(\zeta_1)\}, \qquad \text{(A.1)}$$

where

$$\zeta_1(\lambda) = (\lambda - i)^{1/2} + \lambda^{1/2}, \quad \zeta_2(\lambda) = (\lambda - i)^{1/2} - \lambda^{1/2}, \quad \zeta_3(\lambda) = \lambda^{1/2} - (\lambda - i)^{1/2} = -\zeta_2(\lambda). \qquad \text{(A.2)}$$

For the definition of these functions, the complex $\lambda$-plane is cut on the whole of the negative imaginary axis and on the positive imaginary axis for $\mathrm{Im}(\lambda) > 1$. Figure A1 shows the domains into which the intersection of the cut $\lambda$-plane with the disc $|\lambda| < R$ is mapped in the complex $\zeta$-plane under the mappings $\lambda \to \zeta = \zeta_k(\lambda)$, for $k = 1,2,3$. It is assumed also that $R >> 1$. Figure A1(a) shows the domain in the $\lambda$-plane, with various points on its boundary labelled $A$, $B$ etc., and figure A1(b) shows the domains in the $\zeta$-plane into which it is mapped, under the conformal transformations $\zeta = \zeta_k(\lambda)$, with the boundary points corresponding to $A$, $B$ etc. labelled $A_k$, $B_k$ etc. The outer curved boundary segments in the $\zeta$-plane are circular with radius $2R^{1/2}$ and the inner curved boundary segments are circular with radius $1/(2R^{1/2})$, asymptotically, as $R \to \infty$. The functions $\ln(\zeta_k)$ are well-defined for each $k$ if the $\zeta$-plane is cut along the negative real axis.

The requisite properties of the functions $G_\pm$ follow immediately. For $G_-(\lambda)$, the branch cut in the lower half-plane is only apparent because $G_-$ is continuous across the cut, and a similar statement applies to the cut in the upper half-plane for $G_+(\lambda)$. Also, it is evident from the figure that, for any $\lambda$ in the cut $\lambda$-plane, $\ln(\zeta_3) - \ln(\zeta_2) = i\pi$, which serves to confirm the decomposition (4.5).

## References

Alcántara, J., de la Fuente, D., Chico, B., Simancas, J., Díaz, I. and Morcillo M. (2017). Marine Atmospheric Corrosion of Carbon Steel: A Review, *Materials (Basel)*, PMC5506973, doi: 10.3390/ma10040406

Ayas, C., Fleck, N.A. and Deshpande, V.S. (2015). Hydrogen embrittlement of a bimaterial, *Mechanics of Materials*, **80**, 193-202. DOI 10.1016/j.mechmat.2014.06.002.

Bordes, M., Davies, P., Cognard, J.-Y., Sohire, L., Sauvant-Moynot, V. and Galy, J. (2009). Prediction of long term strength of adhesively bonded steel/epoxy joints in sea water, *Int. J. Adhesion and Adhesives*, **29** 595-608.

Carrier, G. F., Krook, M. and Pearson, C.E. (2005). Functions of a complex variable: theory and technique. Classics in Applied mathematics, SIAM press.

Gettings, M., Baker, F.S. and Kinloch A.J. (1977). Use of Auger and X-ray photoelectron Spectroscopy to study the locus of failure of structural adhesive joints. J. Applied Polymer Sci., **21**, pp. 2375-2392.

**Figure captions**

Fig. 1. Progressive corrosion of an interface by migration of solute from the corrosion zone (rust) on the right-hand side of interface into the upper half-space (epoxy), followed by diffusion within the half-space and then reaction with the lower half-plane (steel) at the pristine, left-hand interface.

Fig. 2. Idealised problem. (a) physical space, with concentration $C$ expressed in terms of stationary co-ordinates $(X,Y)$ and moving co-ordinates $(\bar{x},\bar{y})$; non-dimensional concentration $\phi$ as a function of non-dimensional, moving co-ordinates $(x,y)$.

Fig. 3. Deformed paths for inverse Fourier transform for (a) $x < 0$ and (b) $x > 0$.

Fig. 4. Sensitivity of velocity parameter $c$ to deposition $q$, for $a = 0, 1$.

Fig. 5. Concentration profile upstream of front on interface $y = 0$. (a) $a = 0$ and $c = 0.001$ to 0.1; (b) $a$ in the range 0 to 100, with $c = 0.01$.

Fig. 6. Contour plot of $\phi(x,y)$ for (a) $a = 0$; (b) $a = 1$. $c$=0.01.

Fig. A1. (a) The intersection of the cut $\lambda$-plane with the disc $|\lambda| = R$, (b) the domains in the $\zeta$-plane into which it is mapped by the mappings $\lambda \to \zeta = \zeta_k(\lambda)$, $k$=1, 2, 3.

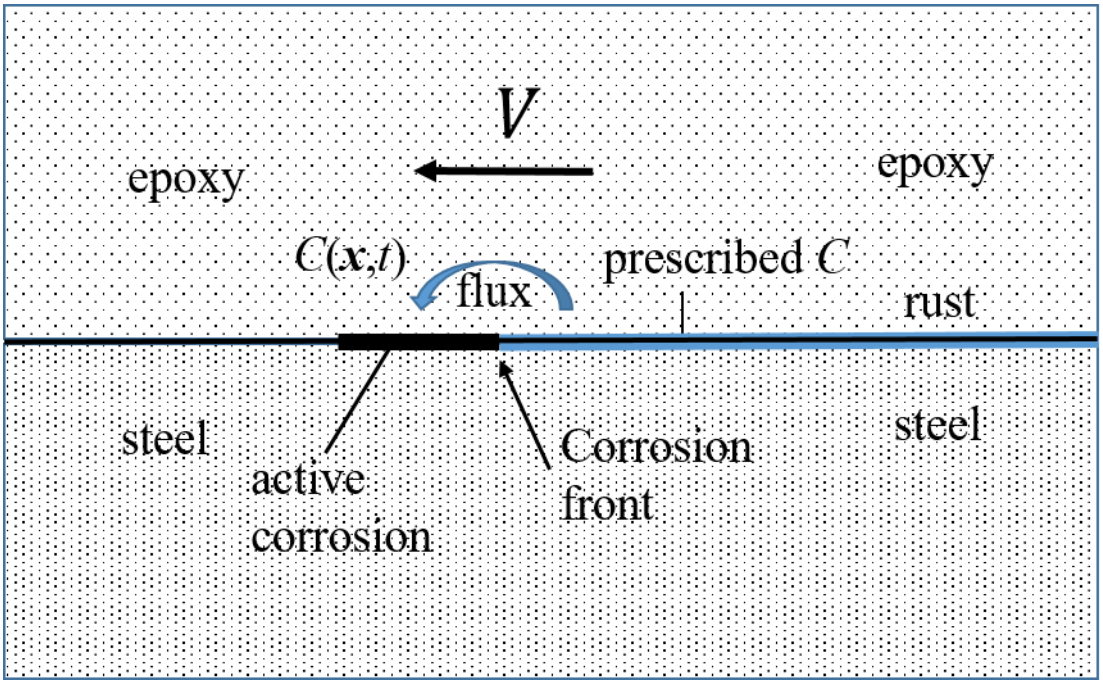


Fig. 1. Progressive corrosion of an interface by migration of solute from the corrosion zone (rust) on the right-hand side of interface into the upper half-space (epoxy), followed by diffusion within the half-space and then reaction with the lower half-plane (steel) at the pristine, left-hand interface.

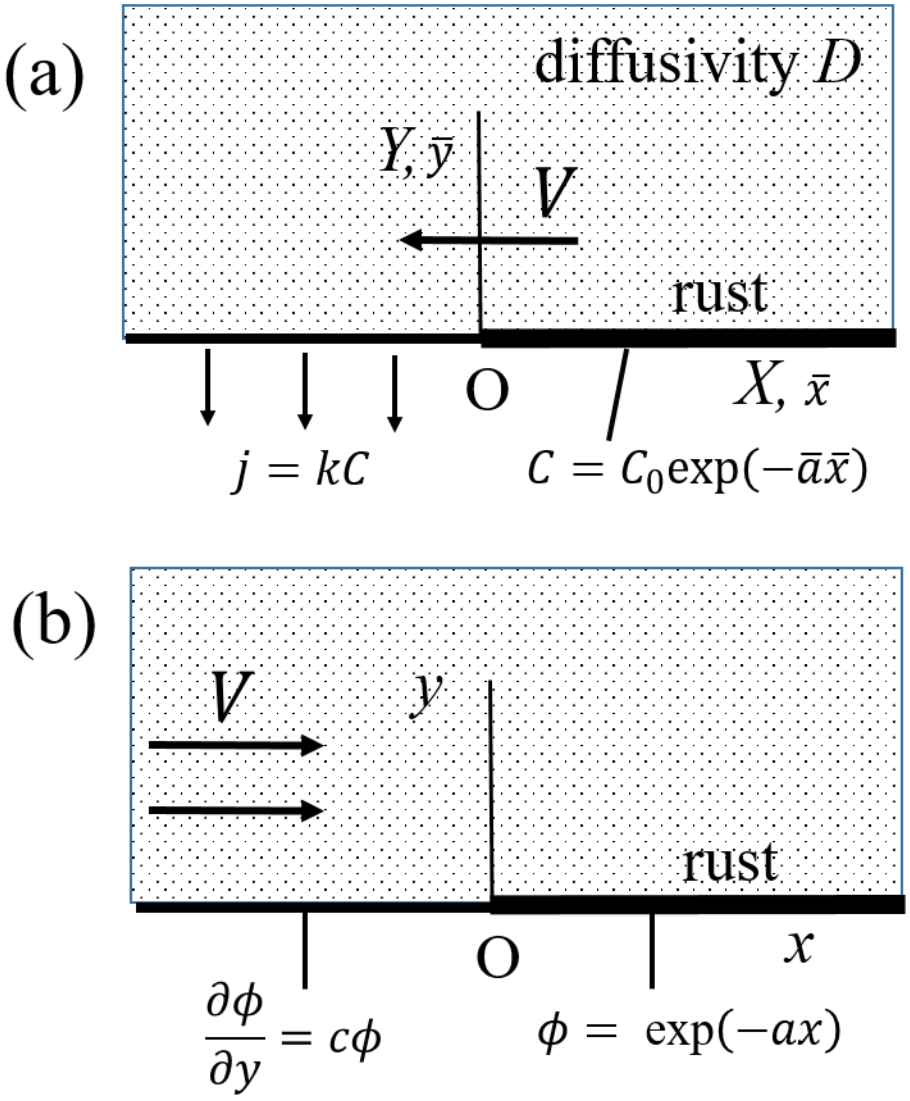


Fig. 2. Idealised problem. (a) physical space, with concentration $C$ expressed in terms of stationary co-ordinates $(X, Y)$ and moving co-ordinates $(\bar{x}, \bar{y})$; non-dimensional concentration $\phi$ as a function of non-dimensional, moving co-ordinates $(x, y)$.

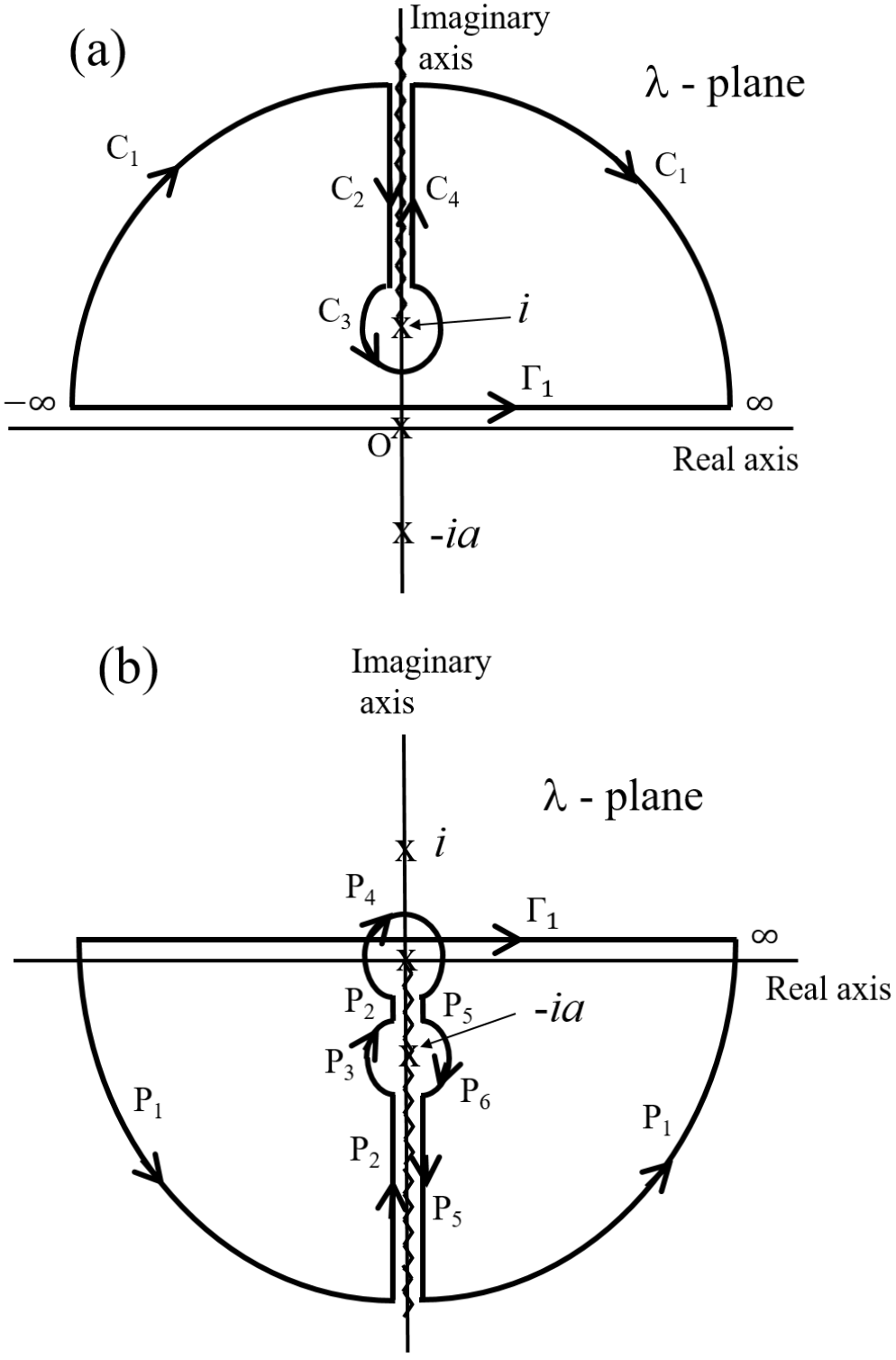


Fig. 3. Deformed paths for inverse Fourier transform for (a) $x < 0$ and (b) $x > 0$.

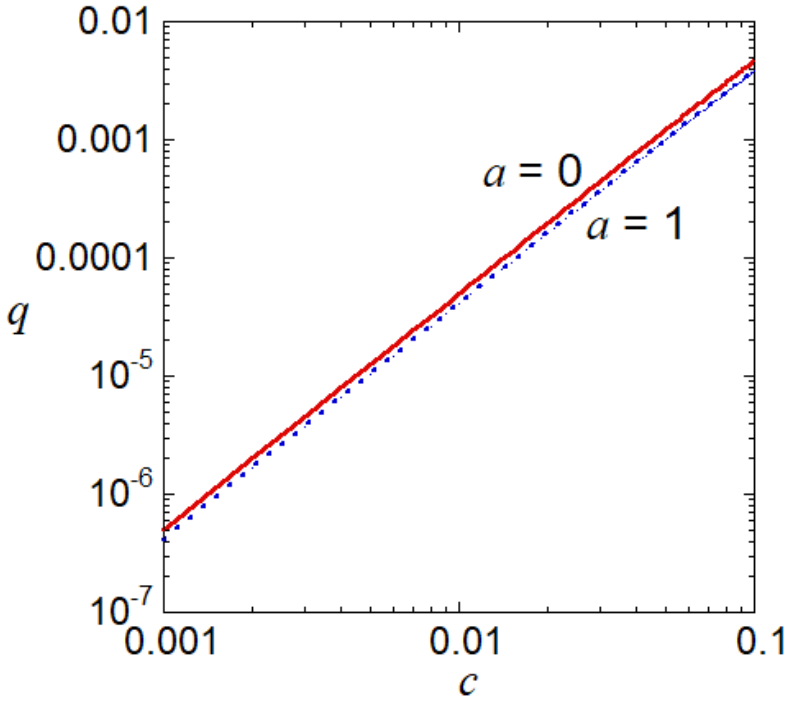


Fig. 4. Sensitivity of velocity parameter $c$ to deposition $q$, for $a = 0, 1$.

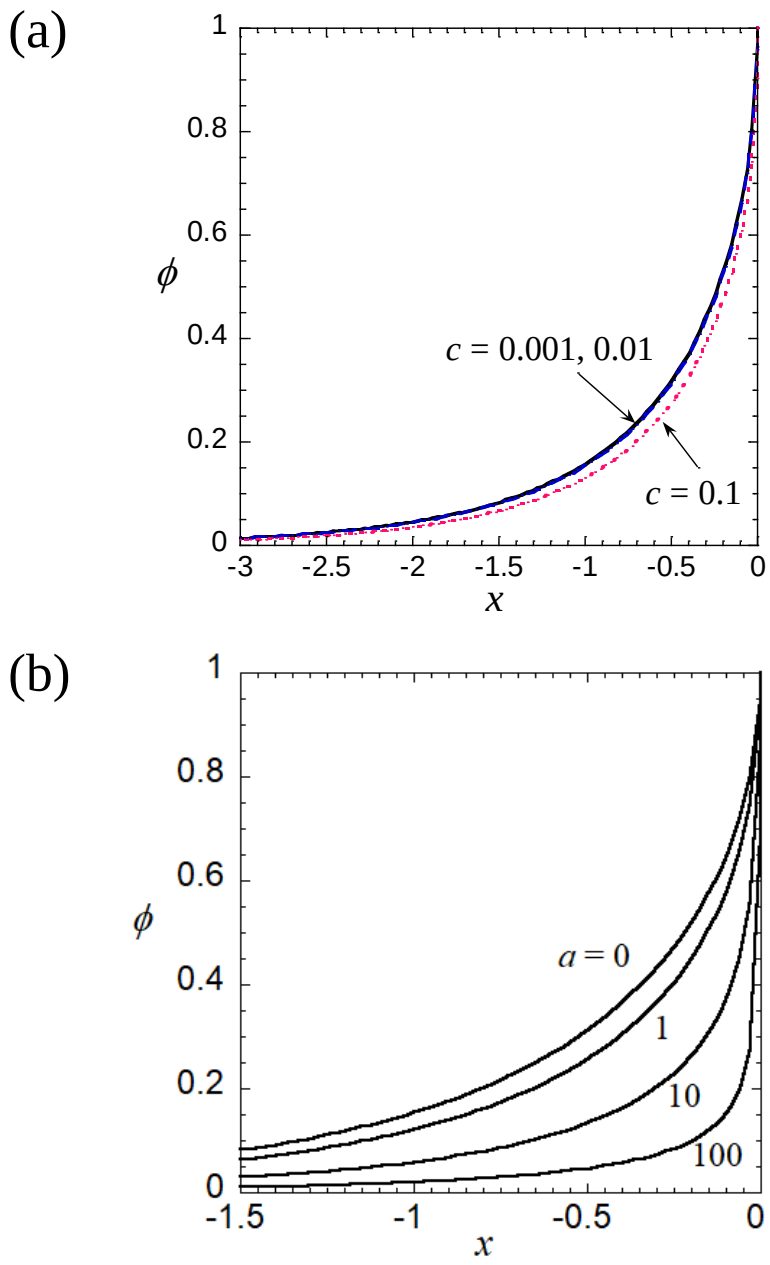


Fig. 5. Concentration profile upstream of front on interface $y = 0$. (a) $a = 0$ and $c = 0.001$ to 0.1; (b) $a$ in the range 0 to 100, with $c = 0.01$.

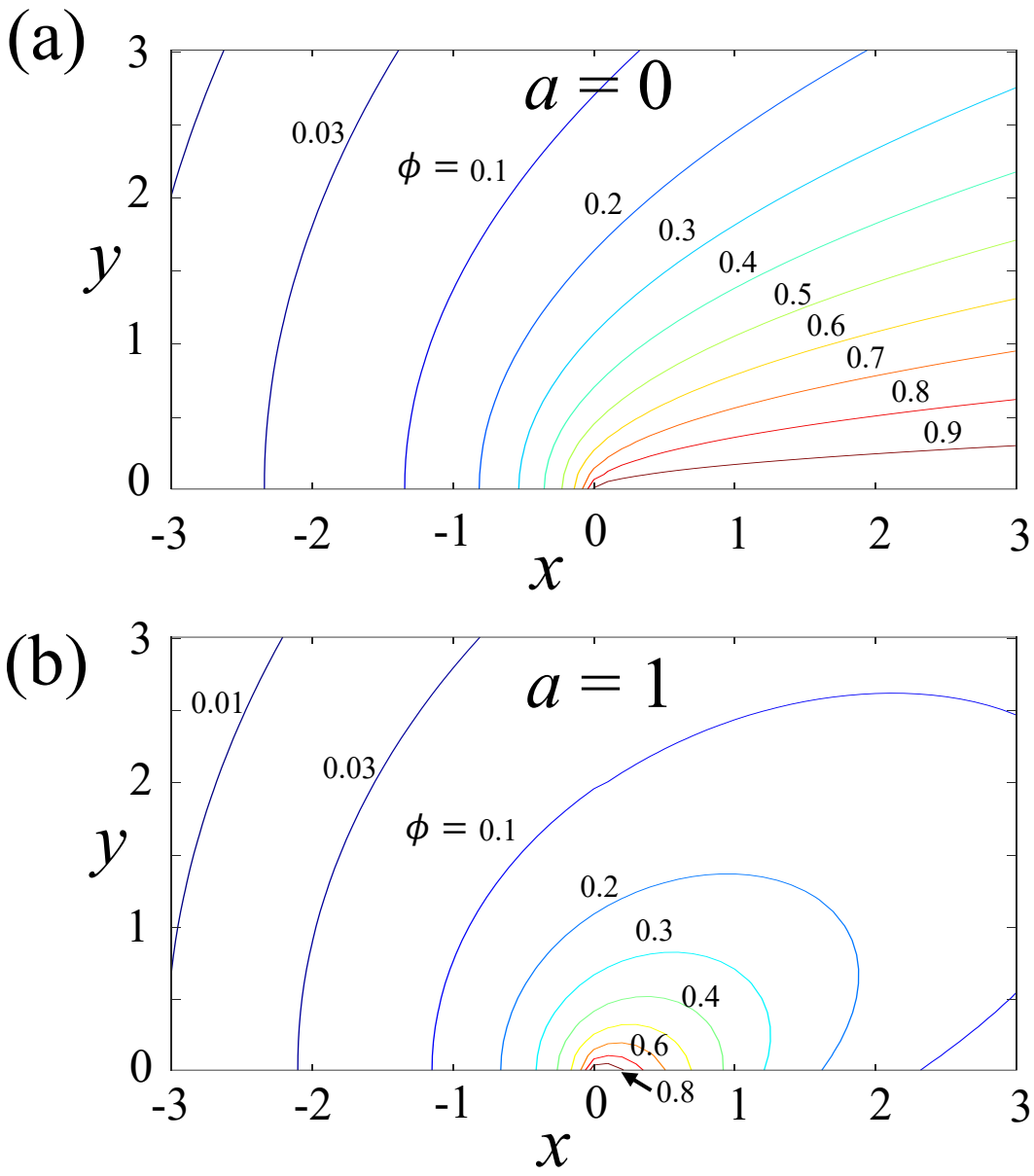


Fig. 6. Contour plot of $\phi(x, y)$ for (a) $a$ = 0; (b) $a$ = 1. $c$=0.01.

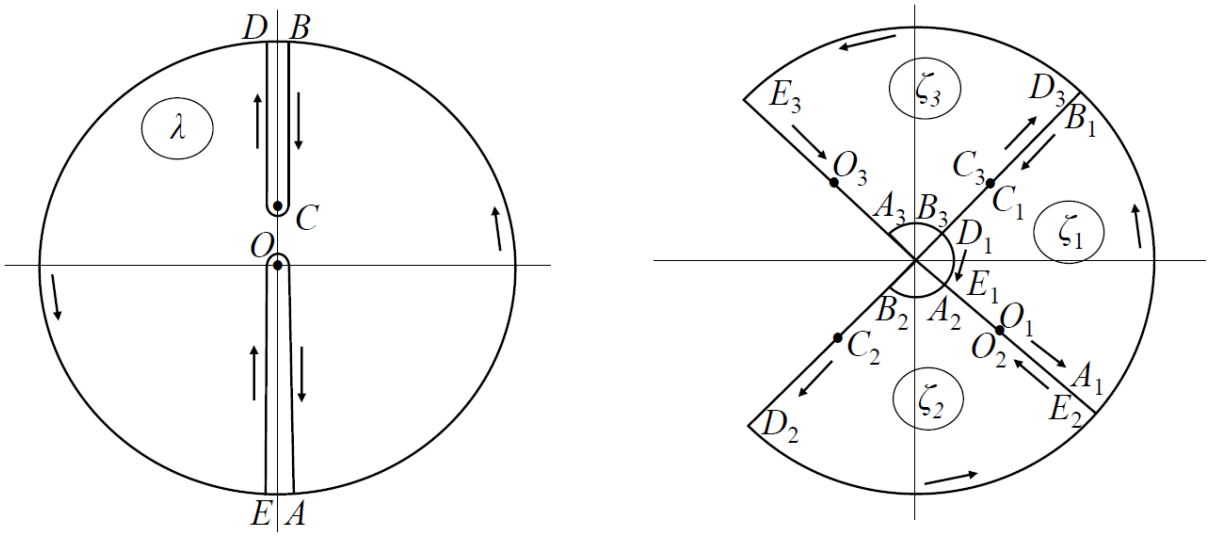


Fig. A1. (a) The intersection of the cut $\lambda$-plane with the disc $|\lambda| = R$, (b) the domains in the $\zeta$-plane into which it is mapped by the mappings $\lambda \to \zeta = \zeta_k(\lambda)$, $k$=1, 2, 3.